Elo, T.; Abhilash, T. S.; Perelshtein, M. R.; Lilja, I.; Korostylev, E. V.; Hakonen, P. J.

Broadband lumped-element Josephson parametric amplifier with single-step lithography

Published in:
Applied Physics Letters

DOI:
10.1063/1.5086091

Published: 15/04/2019

Document Version
Publisher's PDF, also known as Version of record

Please cite the original version:
Elo, T., Abhilash, T. S., Perelshtein, M. R., Lilja, I., Korostylev, E. V., & Hakonen, P. J. (2019). Broadband lumped-element Josephson parametric amplifier with single-step lithography. *Applied Physics Letters*, *114*(15), 1-4. Article 152601. https://doi.org/10.1063/1.5086091

Applied Physics Letters

Broadband lumped-element Josephson parametric amplifier with single-step lithography

Cite as: Appl. Phys. Lett. **114**, 152601 (2019); https://doi.org/10.1063/1.5086091
Submitted: 18 December 2018 . Accepted: 28 March 2019 . Published Online: 15 April 2019

T. Elo, T. S. Abhilash, M. R. Perelshtein, I. Lilja, E. V. Korostylev, and P. J. Hakonen

Applied Physics Letters ARTICLE scitation.org/journal/apl

Broadband lumped-element Josephson parametric amplifier with single-step lithography

Cite as: Appl. Phys. Lett. **114**, 152601 (2019); doi: 10.1063/1.5086091
Submitted: 18 December 2018 · Accepted: 28 March 2019 ·
Published Online: 15 April 2019

T. Elo,[1,a)] T. S. Abhilash,[1] M. R. Perelshtein,[1,2] I. Lilja,[1] E. V. Korostylev,[2] and P. J. Hakonen[1,a)]

AFFILIATIONS

[1]Low Temperature Laboratory, Department of Applied Physics, Aalto University School of Science, P.O. Box 15100, FI-00076 Aalto, Finland
[2]Moscow Institute of Physics and Technology, Moscow 141700, Russian Federation

[a)]**Authors to whom correspondence should be addressed:** teemu.elo@aalto.fi and pertti.hakonen@aalto.fi

ABSTRACT

We present a lumped-element Josephson parametric amplifier (JPA) fabricated using a straightforward e-beam lithography process. Our strongly coupled flux-pumped JPA achieves a gain of 20 dB with a bandwidth of 95 MHz around 5 GHz, while the center frequency is tunable by more than 1 GHz, with the additional possibility for rapid tuning by varying the pump frequency alone. Analytical calculations based on the input-output theory reproduce our measurement results closely.

Low-noise amplification of microwave signals is a key requirement in numerous experiments in quantum technology, including qubit readout, optomechanics, and quantum sensors. Since current state-of-the-art semiconductor amplifiers add 1–3 K of noise to the measured signal,[1] Josephson parametric amplifiers (JPAs),[2,3] along with other superconducting amplifiers,[4–7] having added noise close to one quantum have gained significant interest. The active component in a JPA is the nonlinear inductance of a Josephson junction (JJ), modulating the resonance frequency of a resonator, in first realizations formed by a transmission line cavity.[8–11] However, the bandwidth of cavity-based JPAs is limited to a few megahertz due to the high quality (Q) factor of the cavity.

To achieve higher bandwidths, a lumped-element JPA was introduced,[12] where the JJ and a capacitor form a parallel LC resonator, maximizing the ratio of Josephson inductance to the total inductance. The behavior of a lumped-element JPA can be tuned over a wide range by changing the coupling strength. Besides the high coupled Q configuration,[13] one can omit the coupling capacitor resulting in a low coupled Q and wide bandwidth[12,14] of up to 100 MHz, which can be increased further by engineering the impedance of the environment.[15,16] However, high-performance JPAs are relatively complicated to fabricate, requiring deposition of low-loss dielectrics for parallel plate capacitors and low-impedance vias[14] or optical lithography for niobium followed by e-beam lithography for two aluminum layers.[13]

We present a lumped-element JPA utilizing a straightforward fabrication process. The JJs, capacitor, flux line, and bonding pads are defined in a single e-beam lithography step followed by double-angle evaporation of aluminum. We employ a bridgeless shadow evaporation technique,[17,18] allowing us to fabricate JJs with high critical currents by increasing the surface area instead of lowering the oxide thickness, which could lead to increased variance of critical currents.

First, we consider the theoretical framework of our lumped-element JPA, operating at frequency ω, consisting of a nonlinear resonator formed by a shunt capacitor and a SQUID which is pumped with external RF magnetic flux through the SQUID at frequency $\omega_p \approx 2\omega$ (three-wave mixing). We chose this operation regime, because for a four-wave mixing (typically with a current pump with $\omega_p \approx \omega$), the large amplitude pump is within the amplification bandwidth, whereas the three-wave mixing process separates the pump tone from the amplified signals, therefore simplifying the practical use of the JPA. We can write down the Hamiltonian of a system under study in the rotating wave approximation[19]

$$\hat{H} = \hbar\xi_r \hat{a}^\dagger \hat{a} - \frac{\hbar}{2}\left[\alpha^* \hat{a}^2 + \alpha \hat{a}^{\dagger 2}\right]. \quad (1)$$

In this formula, $\xi_r = \omega_p/2 - \omega_r$, where ω_r is the resonator frequency, α is the strength of the pump, and $\hat{a}$ is the cavity mode. Solving the Quantum Langevin Equation (QLE) with the Hamiltonian above yields the signal gain as a function of frequency. In QLE, we take into consideration a cavity decay rate κ, which is determined by the JPA quality factor Q: $\kappa = \omega/Q$. Since our JPA is strongly coupled to the environment, its quality factor is dominated by coupling, and

therefore, $Q \approx Q_c\left(= Z_0\sqrt{C/L}\right)$. The resulting amplification of the signal at frequency ω as a function of detuning $\xi = \omega_p/2 - \omega$ is given by

$$G(\xi) = \left|1 - \frac{\kappa\chi\left(\frac{\omega_p}{2} + \xi\right)}{1 - |\alpha|^2\chi\left(\frac{\omega_p}{2} + \xi\right)\chi^*\left(\frac{\omega_p}{2} - \xi\right)}\right|^2, \quad (2)$$

where $\chi(\omega) = [\kappa/2 - i(\omega - \omega_r)]^{-1}$ is the electrical susceptibility of the resonator. It can be seen from the equation that gain is achieved at various resonator detunings, but to clarify this dependence, we fix the pump power to $\alpha_{\max} = \kappa/2$, corresponding to infinite gain at zero detuning. Now, by substituting $\chi = (\kappa/2 - i\sigma\kappa)^{-1}$, where we introduce $\sigma = \xi_r/\kappa$, the maximum gain at a given resonator detuning is given by

$$G(\sigma) = \frac{(1 + 2\sigma^2)^2}{4\sigma^2(1 + \sigma^2)}. \quad (3)$$

In the high-gain limit, we can assume that $\xi_r \ll \kappa$, and in terms of quality factor, this relation can be written as $G = |2Q\xi_r/\omega_r|^{-2}$. Consequently, we can express the pump frequency range where the gain exceeds a given value G_0

$$\omega_p(G_0) = \omega_r\left(2 \pm \frac{1}{\sqrt{G_0}\,Q}\right). \quad (4)$$

Then, in addition to the wide bandwidth, JPA with a low quality factor has the advantage of wide tunability by varying the pump frequency. This tuning via ω_p is a considerably faster operation than changing the DC flux value. This rapid tuning would be beneficial in various frequency-multiplexing schemes, e.g., in sequential readout of resonators at different frequencies. If the JPA frequency switching time is sufficiently short, multiple resonators can be measured before the ringdown of the resonators. In general, when the pump power is not fixed, it is possible to use $\eta = \alpha/\alpha_{\max} = 2\,\alpha/\kappa$ to evaluate the final maximum gain function of the two parameters controlled in the experiment

$$G(\sigma, \eta) = \frac{(\eta^2 + 4\sigma^2 + 1)^2}{\eta^4 + \eta^2(8\sigma^2 - 2) + (4\sigma^2 + 1)^2}, \quad (5)$$

where $\eta \leq 1$. Here, if $\eta = 1$, this equation turns into Eq. (3). Note that in the case $\sigma = 0$, meaning zero resonator detuning, gain tends to infinity.

The design of our JPA is shown in Fig. 1. The layout design follows a lumped-element principle: no transmission lines are required since all distances are kept short compared to the wavelength ($\lambda \approx 30$ mm at 10 GHz). Instead of a ground plane spreading over the entire chip, we place the SQUID and the capacitor in proximity to two bonding pads. The JPA is tuned and pumped with an external AC + DC flux through the SQUID loop, applied with an excitation line whose geometry is designed to reduce parasitic coupling to the loop formed by the SQUID and the capacitor.

While the resonance frequency of the JPA is given by $\omega_p = 1/\sqrt{LC}$, the amplification bandwidth is inversely proportional to quality factor $Q = Z_0\sqrt{C/L}$[15,16] and thus related to critical current of the SQUID as $1/I_c$. On the other hand, the saturation power of the JPA is directly proportional to I_c, resulting in a trade-off between the bandwidth and saturation power. Moreover, JPAs with low Q require strong pumping, which may cause unwanted nonlinear behavior.[16,20] However, in our application, a wide bandwidth is preferred over high saturation power, and therefore, we set $Q \approx 2$, resulting in $C = 1.2$ pF and $L = 0.8$ nH, obtained by applying a DC magnetic flux of $\Phi_{DC} \approx 0.4\Phi_0$ through a SQUID with a total unbiased of $I_c = 1.2\ \mu$A.

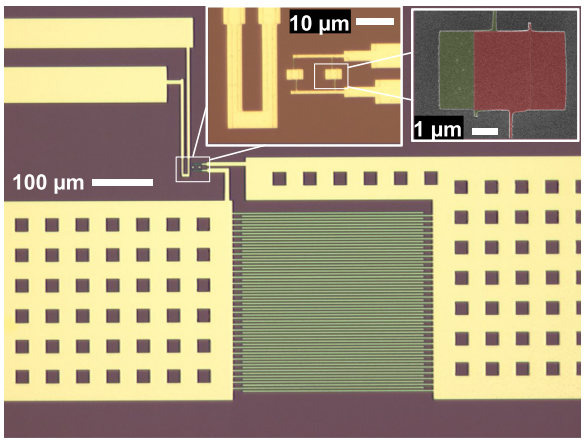

FIG. 1. Micrographs of a fabricated JPA. Main figure and top-middle inset: Optical micrographs of the JPA. Top-right inset: false-color SEM image of a fabricated Josephson junction with green and red colors denoting first and second aluminum layers, respectively.

The capacitor was realized as an interdigital capacitor due to its low losses[21] and good suitability to our e-beam lithography process. The capacitor is oriented so that the rotational axis of evaporation angles is perpendicular to the capacitor fingers, allowing proper control over the finger widths. The 1.2 pF capacitor has 62 fingers with a length of 330 μm and a width and a gap of 2.4 μm, connected to the bonding pads directly, thus minimizing parasitic inductance. Since large interdigital capacitors may exhibit nonideal behavior at high frequencies, we verified our capacitor design with electromagnetic (EM) simulations.[22] In addition, EM simulations were used to estimate the total geometric inductance of the JPA device, resulting in less than 10% of the total inductance in the operating range.

For the Josephson junctions, we chose a small critical current density (7 A/cm^2) to improve the quality and reproducibility of the JJs. This, combined with the 600 nA critical current of the JJs, results in a junction area of $\sim 9\ \mu$m^2. Since such JJs are difficult to fabricate using the Dolan bridge technique, we employed a bridgeless shadow evaporation process,[17] where the layer separation is realized in the leads connecting the JJs: the lines leading up- and downwards from the JJ in Fig. 1 are formed by the first and second aluminum layers, respectively. We have also fabricated similar JPAs using the bridge technique using higher critical current density.

The JPAs were fabricated on an oxidized silicon substrate by e-beam lithography using double layer resist [Copolymer methyl methacrylate - methacrylic acid (MMA-MAA) 700 nm + PMMA 200 nm] and a 100 kV beam to achieve low parasitic undercuts although 20 kV is also feasible if e-beam doses are well-adjusted.[17,23] The process involved a double-angle ($\pm 45°$) evaporation of 75 nm thick aluminum, separated by *in-situ* oxidation at 15 mbar for 10 min.

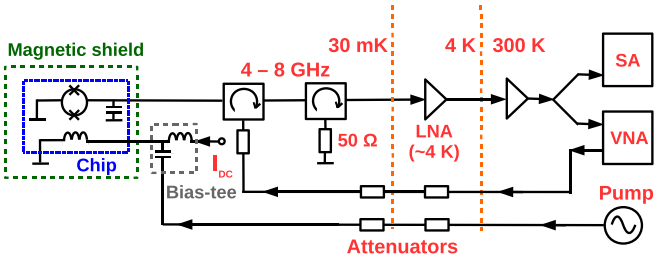

FIG. 2. Simplified schematic of the measurement system used in characterization of the JPA. The transmission measurements were conducted using a vector network analyzer (VNA), while a spectrum analyzer (SA) was used for noise measurements.

Our measurement setup is illustrated in Fig. 2. The measurements were conducted at 30 mK using a BlueFors LD-250 dry dilution cryostat. The JPA was protected from external magnetic fields with a cylindrical Cryoperm shield and a superconducting (Pb) inner shield. The DC flux bias and the RF pump shared a common on-chip flux line, and the signals were combined by an external bias-tee.

First, we characterized the tunability of the JPA resonance frequency as a function of DC magnetic flux applied through the SQUID loop. Fig. 3 shows the phase of the reflected signal and the calculated estimates for resonance frequency using both the ideal and EM-simulated capacitor model including parasitic inductance. Although our capacitor contains parasitics, we observe that at the desired working point at 5 GHz, the deviation between the two capacitor models is negligible, meaning that the capacitor can be considered nearly ideal at those frequencies.

We then characterized the JPA gain at various values of Φ_{DC}. Our JPA exhibited >13 dB gain at $0.3\ \Phi_0 < \Phi_{DC} < 0.4\ \Phi_0$, and the widest tunability was obtained at $\Phi_{DC} = 0.36\ \Phi_0$. The maximum gain at that point is plotted in Fig. 4 as a function of pump frequency and pump power entering the JPA, omitting reflection and finite coupling of the pump tone to the SQUID. The observed variation of the pump power at maximum gain was most likely caused by minor resonances in the flux pumping line, causing the actual RF flux amplitude through the SQUID to fluctuate as a function of the pump frequency at constant applied pump power. It should be noted that the operation frequency can be tuned by several hundred megahertz varying the pump frequency alone, as shown in Eq. (4), while additional tunability from 4.8 to 5.8 GHz can be achieved by varying the DC flux as well.

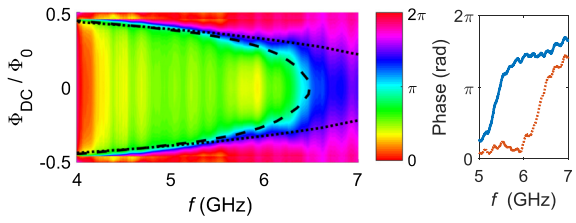

FIG. 3. Left: Phase of the reflected signal as a function of frequency and applied DC flux. The dotted and dashed lines are the estimated JPA resonances using ideal and EM-simulated dispersive capacitor models, respectively. Right: Line cuts at $\Phi_{DC} = 0.36\ \Phi_0$ (blue curve) and at $\Phi_{DC} = 0$ (red dotted curve).

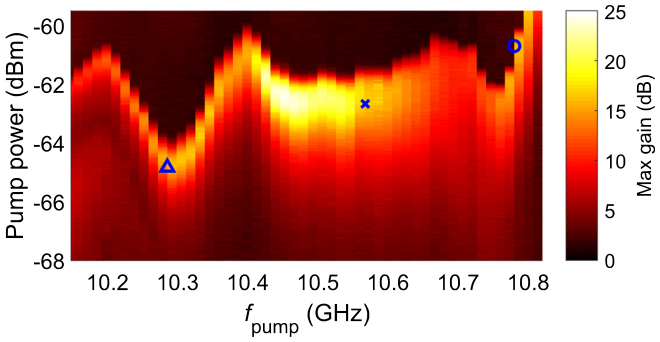

FIG. 4. Maximum value of the measured gain as a function of pump frequency and power at $\Phi_{DC} = 0.36\ \Phi_0$. The corresponding linear resonance frequency is 5.3 ± 0.1 GHz. The blue markers denote operating points in Fig. 5.

Noise performance of the JPA was characterized using the signal-to-noise ratio (SNR) improvement method, giving noise relative to system noise temperature, which was calibrated separately using the Y-factor method with a heated load. Thus, we can estimate the noise temperature of the JPA using the following relation:[16]

$$T_{JPA}(\omega) = T_{tot}(\omega)\left(\frac{1}{\eta_{SNR}(\omega)} - \frac{1}{G(\omega)}\right), \tag{6}$$

where $T_{tot}(\omega)$ is the total system noise referred to the JPA input port including the noise of the HEMT preamplifier and losses in cables and circulators, $\eta_{SNR}(\omega)$ is the SNR improvement, and $G(\omega)$ is the gain as defined in Eq. (2). Our system noise has a mean value of about 6 K.

The gain and noise characteristics of the JPA in the denoted operating points are shown in Fig. 5. The dashed red line marks the calculated gain outline, showing good agreement with the experiment. In calculations, we used $\Phi_{DC} = 0.36\ \Phi_0$ for DC flux and $\Phi_{RF} = 0.07\ \Phi_0$

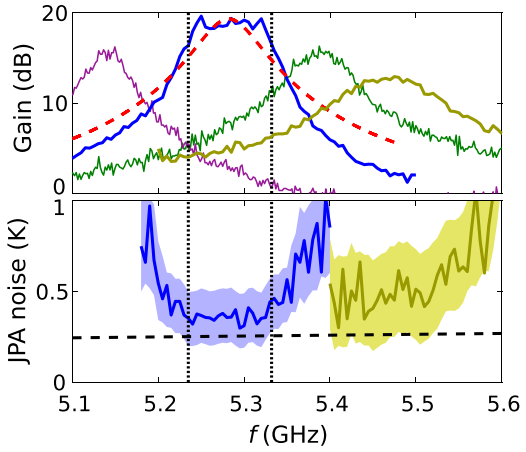

FIG. 5. Measured gain (upper) and noise (lower) of the JPA at various pump parameters at $\Phi_{DC} = 0.36\Phi_0$. The operation points for magenta, blue, and green curves are marked with a triangle, cross, and circle in Fig. 4, respectively. The vertical lines denote the −3 dB bandwidth of 95 MHz for the blue curve. For yellow curves, $f_{pump} = 10.927$ GHz and $P_{pump} = -62.2$ dBm. In the noise plot, the shaded areas denote the measurement error, while the dashed line represents the standard quantum limit ($T_Q = \hbar\omega/k_B$).

for RF flux, and the strength of the pump was 0.45 κ (= 0.9 α_{max}). The observed 20 dB gain with a bandwidth of 95 MHz is of the same order as reported previously for a strongly coupled lumped-element JPA.[14] The noise performance approaches the quantum limit ($T_Q = \hbar\omega/k_B$) within the measurement error, as expected for a low-loss JPA. We attribute the large error to the inaccuracies in cable losses and the system noise temperature measurement. Since our design was optimized for the wide bandwidth, the determined input power resulting in 1 dB gain compression was -125 ± 3 dBm, which, although low, is adequate for various experiments. One example is measurements of low-bias shot noise, with noise powers equivalent to a few millidegrees Kelvin, which currently require long integration times with HEMT amplifiers.[24] Additionally, the saturation power is sufficient for superconducting qubit readout, where a typical photon occupation in a readout resonator $\langle n \rangle = 3$ with effective $Q = 1000$ corresponds to a probe power of $P \approx -130$ dBm.[25,26]

In summary, we have designed and fabricated a JPA using a straightforward fabrication process with single-step e-beam lithography. The design favoring a wide bandwidth over a high dynamic range resulted in nearly quantum-limited noise performance with a gain of 20 dB and a bandwidth of 95 MHz, which will be useful, e.g., in shot noise spectroscopy, qubit readout, and quantum vacuum measurements,[27,28] where signal levels are low. Varying the pump frequency allows rapid tuning of the JPA band center by several hundred megahertz. Because the JPA is relatively simple to fabricate, the design can be easily modified to meet the requirements of various experimental settings. These modifications include, for example, having additional SQUID loops in series to enhance the saturation power[18] or placing an impedance-matching waveguide structure either on- or off-chip to improve the amplification bandwidth.[15,16]

We thank A. Lebedev and S. Paraoanu for fruitful discussions. This work was financially supported by the Academy of Finland (Projects Nos. 314448 and 312295), by ERC (Grant No. 670743), by the Centre for Quantum Engineering at Aalto University, by the Government of the Russian Federation (Agreement 05.Y09.21.0018), by Foundation for the Advancement of Theoretical Physics and Mathematics "BASIS", and by the Ministry of Education and Science of the Russian Federation (Grant Nos. RFMEFI59417X0014 and 16.7162.2017/8.9). T.E. is grateful to Väisälä Foundation of the Finnish Academy of Science and Letters for scholarship. This research work made use of the Aalto University OtaNano/LTL infrastructure which is part of the European Microkelvin Platform funded by European Union's Horizon 2020 Research and Innovation Programme under Grant Agreement No. 824109. Our project also took advantage of equipment at the MIPT Shared Facilities Center.

REFERENCES

[1]J. Schleeh, G. Alestig, J. Halonen, A. Malmros, B. Nilsson, P. A. Nilsson, J. P. Starski, N. Wadefalk, H. Zirath, and J. Grahn, IEEE Electron Device Lett. **33**, 664 (2012).
[2]H. Zimmer, Appl. Phys. Lett. **10**, 193 (1967).
[3]B. Yurke, P. G. Kaminsky, R. E. Miller, E. A. Whittaker, A. D. Smith, A. H. Silver, and R. W. Simon, Phys. Rev. Lett. **60**, 764 (1988).
[4]B. Ho Eom, P. K. Day, H. G. Leduc, and J. Zmuidzinas, Nat. Phys. **8**, 623 (2012).
[5]P. Lähteenmäki, V. Vesterinen, J. Hassel, H. Seppä, and P. Hakonen, Sci. Rep. **2**, 276 (2012).
[6]P. Lähteenmäki, V. Vesterinen, J. Hassel, G. S. Paraoanu, H. Seppä, and P. Hakonen, J. Low Temp. Phys. **175**, 868 (2014).
[7]S. Jebari, F. Blanchet, A. Grimm, D. Hazra, R. Albert, P. Joyez, D. Vion, D. Estève, F. Portier, and M. Hofheinz, Nat. Electron. **1**, 223 (2018).
[8]T. Yamamoto, K. Inomata, M. Watanabe, K. Matsuba, T. Miyazaki, W. D. Oliver, Y. Nakamura, and J. S. Tsai, Appl. Phys. Lett. **93**, 042510 (2008).
[9]M. A. Castellanos-Beltran, K. D. Irwin, G. C. Hilton, L. R. Vale, and K. W. Lehnert, Nat. Phys. **4**, 929 (2008).
[10]N. Bergeal, F. Schackert, M. Metcalfe, R. Vijay, V. E. Manucharyan, L. Frunzio, D. E. Prober, R. J. Schoelkopf, S. M. Girvin, and M. H. Devoret, Nature **465**, 64 (2010).
[11]M. Simoen, C. W. S. Chang, P. Krantz, J. Bylander, W. Wustmann, V. Shumeiko, P. Delsing, and C. M. Wilson, J. Appl. Phys. **118**, 154501 (2015).
[12]M. Hatridge, R. Vijay, D. H. Slichter, J. Clarke, and I. Siddiqi, Phys. Rev. B **83**, 134501 (2011).
[13]X. Zhou, V. Schmitt, P. Bertet, D. Vion, W. Wustmann, V. Shumeiko, and D. Esteve, Phys. Rev. B **89**, 214517 (2014).
[14]J. Y. Mutus, T. C. White, E. Jeffrey, D. Sank, R. Barends, J. Bochmann, Y. Chen, Z. Chen, B. Chiaro, A. Dunsworth, J. Kelly, A. Megrant, C. Neill, P. J. J. O'Malley, P. Roushan, A. Vainsencher, J. Wenner, I. Siddiqi, R. Vijay, A. N. Cleland, and J. M. Martinis, Appl. Phys. Lett. **103**, 122602 (2013).
[15]J. Y. Mutus, T. C. White, R. Barends, Y. Chen, Z. Chen, B. Chiaro, A. Dunsworth, E. Jeffrey, J. Kelly, A. Megrant, C. Neill, P. J. J. O'Malley, P. Roushan, D. Sank, A. Vainsencher, J. Wenner, K. M. Sundqvist, A. N. Cleland, and J. M. Martinis, Appl. Phys. Lett. **104**, 263513 (2014).
[16]T. Roy, S. Kundu, M. Chand, A. M. Vadiraj, A. Ranadive, N. Nehra, M. P. Patankar, J. Aumentado, A. A. Clerk, and R. Vijay, Appl. Phys. Lett. **107**, 262601 (2015).
[17]F. Lecocq, I. M. Pop, Z. Peng, I. Matei, T. Crozes, T. Fournier, C. Naud, W. Guichard, and O. Buisson, Nanotechnology **22**, 315302 (2011).
[18]L. Planat, R. Dassonneville, J. P. Martinez, F. Foroughi, O. Buisson, W. Hasch-Guichard, C. Naud, R. Vijay, K. Murch, and N. Roch, Phys. Rev. Appl. **11**, 034014 (2019).
[19]P. Lähteenmäki, G. S. Paraoanu, J. Hassel, and P. J. Hakonen, Proc. Natl. Acad. Sci. **110**, 4234 (2013).
[20]V. E. Manucharyan, E. Boaknin, M. Metcalfe, R. Vijay, I. Siddiqi, and M. Devoret, Phys. Rev. B **76**, 014524 (2007).
[21]I. Bahl, *Lumped Elements for RF and Microwave Circuits* (Artech House, Norwood, MA, USA, 2003).
[22]CST Microwave Studio and Sonnet were used for EM simulations.
[23]J. S. Penttilä, Ü. Parts, P. J. Hakonen, M. A. Paalanen, and E. B. Sonin, Phys. Rev. Lett. **82**, 1004 (1999).
[24]T. Nieminen, P. Lähteenmäki, Z. Tan, D. Cox, and P. J. Hakonen, Rev. Sci. Instrum. **87**, 114706 (2016).
[25]Z. R. Lin, K. Inomata, W. D. Oliver, K. Koshino, Y. Nakamura, J. S. Tsai, and T. Yamamoto, Appl. Phys. Lett. **103**, 132602 (2013).
[26]J. Heinsoo, C. K. Andersen, A. Remm, S. Krinner, T. Walter, Y. Salathé, S. Gasparinetti, J.-C. Besse, A. Potočnik, A. Wallraff, and C. Eichler, Phys. Rev. Appl. **10**, 034040 (2018).
[27]L. Zhong, E. P. Menzel, R. Di Candia, P. Eder, M. Ihmig, A. Baust, M. Haeberlein, E. Hoffmann, K. Inomata, T. Yamamoto, Y. Nakamura, E. Solano, F. Deppe, A. Marx, and R. Gross, New J. Phys. **15**, 125013 (2013).
[28]P. Lähteenmäki, G. S. Paraoanu, J. Hassel, and P. J. Hakonen, Nat. Commun. **7**, 12548 (2016).